Journal of Non-Newtonian Fluid Mechanics 260 (2018) 76–86

Contents lists available at ScienceDirect

Journal of Non-Newtonian Fluid Mechanics

journal homepage: www.elsevier.com/locate/jnnfm

Lubrication solution of the axisymmetric Poiseuille flow of a Bingham fluid with pressure-dependent rheological parameters

Kostas D. Housiadas[a], Iasonas Ioannou[b], Georgios C. Georgiou[b,*]

[a] Department of Mathematics, University of the Aegean, Karlovassi, Samos 83200, Greece
[b] Department of Mathematics and Statistics, University of Cyprus, P.O. Box 20537, Nicosia 1678, Cyprus

ARTICLE INFO

Keywords:
Bingham plastic
axisymmetric Poiseuille flow
pressure-dependent viscosity
pressure-dependent yield stress
lubrication solution

ABSTRACT

The lubrication flow of a Bingham plastic in long tubes is modeled using the approach proposed by Fusi and Farina (Appl. Math. Comp. 320, 1–15 (2018)). Both the plastic viscosity and the yield stress are assumed to vary linearly with the total pressure. The resulting nonlinear system of an ordinary differential equation and an algebraic one with unknowns the total pressure and the radius of the unyielded core are solved by using two different techniques. A pseudospectral numerical method utilizing Chebyshev orthogonal polynomials and an analytical perturbation method with the small parameter being the difference of the two dimensionless parameters which are introduced due to the pressure-dependence of the yield stress and the plastic viscosity of the material. The effects of the pressure-dependence of the material parameters on the critical pressure difference required for flow to occur and on the shape of the unyielded core are investigated and discussed.

1. Introduction

We consider the axisymmetric Poiseuille flow of a Bingham plastic [1] with pressure-dependent rheological parameters. More specifically, we consider the flow in long horizontal tubes of yield-stress materials with pressure-dependent yield stress, $\tau_y^* = \tau_y^*(p^*)$, and plastic viscosity, $\mu^* = \mu^*(p^*)$, where p^* is the pressure. Hence, the constitutive equation can be written in tensorial form as follows:

$$\begin{cases} \dot{\boldsymbol{\gamma}}^* = 0, & \tau^* \le \tau_y^*(p^*) \\ \boldsymbol{\tau}^* = \left[\dfrac{\tau_y^*(p^*)}{\dot{\gamma}^*} + \mu^*(p^*) \right] \dot{\boldsymbol{\gamma}}^*, & \tau^* > \tau_y^*(p^*) \end{cases} \tag{1}$$

where $\boldsymbol{\tau}^*$ is the viscous extra-stress tensor and $\dot{\boldsymbol{\gamma}}^*$ is the rate-of-deformation tensor:

$$\dot{\boldsymbol{\gamma}}^* = \nabla^* \mathbf{v}^* + \left(\nabla^* \mathbf{v}^*\right)^T \tag{2}$$

In Eqs. (1) and (2), $\mathbf{v}^*$ is the velocity vector and $\dot{\gamma}^* \equiv \sqrt{\mathrm{tr}(\dot{\boldsymbol{\gamma}}^* \cdot \dot{\boldsymbol{\gamma}}^*)/2}$ and $\tau^* \equiv \sqrt{\mathrm{tr}(\boldsymbol{\tau}^* \cdot \boldsymbol{\tau}^*)/2}$ are the magnitudes of $\dot{\boldsymbol{\gamma}}^*$and $\boldsymbol{\tau}^*$, respectively. Eq. (1) is a generalization of the classical Bingham-plastic equation, which is recovered when both τ_y^* and μ^* are constant (pressure-independent). This reduces to the Newtonian constitutive equation by setting $\tau_y^* = 0$, μ^* thereby being the familiar Newtonian viscosity. It should be noted that throughout this paper starred symbols denote dimensional quantities.

The axisymmetric Poiseuille flow of a material obeying Eq. (1) is of interest in the transport of such materials in long tubes, where high pressures are required to drive the flow, e.g. in oil-drilling. Experimental data showed that oil-drilling fluids are indeed viscoplastic and their rheological parameters vary not only with temperature but also with pressure [2]. Hermoso et al. [2] reported experimental data at different pressures and temperatures for the rheological behavior of two oil-based drilling fluids, obeying the Bingham-plastic and the Herschel-Bulkley models (the latter generalizes the former model introducing the power-law exponent as an additional parameter) [3]. This data showed that at low temperatures the yield stress decreases with temperature and increases with pressure and that both variations are linear. In order to model the isothermal yield stress behaviour of the two drilling fluids, Hermoso et al. [2] employed the following linear equation

$$\tau_y^*(p^*) = \tau_0^* \left[1 + \beta^*(p^* - p_0^*)\right] \tag{3}$$

where τ_0^* denotes the yield stress at a reference pressure p_0^* and β^* is the yield-stress growth coefficient. As for the plastic viscosity (of the fluid obeying the Bingham plastic equation), they used the Barus equation

$$\mu^*(p^*) = \mu_0^* \, \mathrm{e}^{\alpha^*(p^* - p_0^*)} \tag{4}$$

where μ_0^* is the plastic viscosity at the reference pressure and $a^* \ge 0$ is the plastic-viscosity growth coefficient [4]. The linearized version of Eq. (4),

$$\mu^*(p^*) = \mu_0^* \left[1 + a^*(p^* - p_0^*)\right] \tag{5}$$

may also been used if the pressure-dependence of μ^* is weak ($a^* << 1$), the encountered pressures are not extremely high and remain always

* Corresponding author.
E-mail address: georgios@ucy.ac.cy (G.C. Georgiou).

https://doi.org/10.1016/j.jnnfm.2018.06.003
Received 27 March 2018; Received in revised form 1 June 2018; Accepted 3 June 2018
Available online 7 July 2018

above the reference pressure [5]. It is clear that the latter limitation also holds for the linear expression (3) for the yield stress.

Damianou and Georgiou [6] analyzed the plane Poiseuille flow of a Bingham plastic of material parameters obeying Eqs. (2) and (4), such that

$$\begin{cases} \dot{\boldsymbol{\gamma}}^* = \mathbf{0}, & \tau^* \le \tau_y^*(p^*) \\ \tau^* = 2\left[\dfrac{\tau_0^*\left[1+\beta^*\left(p^*-p_0^*\right)\right]}{\dot{\gamma}^*} + \mu_0^*\left[1+\alpha^*\left(p^*-p_0^*\right)\right]\right]\dot{\boldsymbol{\gamma}}^*, & \tau^* > \tau_y^*(p^*) \end{cases} \tag{6}$$

and reported explicit analytical solutions for the velocity, the pressure, and the width of the central unyielded region. It turns out that the latter is constant despite the pressure-dependence of the material parameters. In axisymmetric Poiseuille flow, however, the radius of the unyielded core is not constant in the general case. As pointed out in Ioannou and Georgiou [7], an analytical solution with a cylindrical unyielded region can be derived only when the growth coefficients α^* and β^* are equal, which is indeed a reasonable assumption for certain oil-drilling fluids. Recently, Fusi and Rosso [8] have obtained analytical solutions of the axisymmetric flow of a Herschel-Bulkley fluid with different values of α^* (growth coefficient of the consistency index) and β^*, under the assumption that both $\alpha^*(p^*-p_0^*)$ and $\beta^*(p^*-p_0^*)$ are much greater than unity. These solutions are not reduced to the classical constant-parameter solutions when α^* and β^* vanish.

Panaseti et al. [5] extended the lubrication-approximation method of Fusi et al. [9] to model the flow of a Herschel-Bulkley fluid in a symmetric long channel of varying width, under the assumption that both the consistency index and the yield stress vary linearly with pressure. In this method, the unyielded domain is modeled as an evolving non-material volume and by means of an integral formulation for the balance of linear momentum a single integro-differential equation is derived for the pressure. The yield surface and the two velocity components are then calculated from the pressure by means of closed form expressions. The main advantages of the method of Fusi et al. [9] are: (a) the yield surface, i.e. the interface between yielded ($\tau^* > \tau_y^*$) and unyielded ($\tau^* \le \tau_y^*$) parts of the flow domain, is calculated exactly; and (b) the so-called lubrication-approximation paradox is avoided and the correct shape of the yield surface, which is opposite to that of the wall, is approximated at zero order, unlike other lubrication-approximation approaches in which higher-order solutions are necessary [10]. A limitation of the method, however, is that it cannot be applied when the plug region is broken, since the plug is required to extend from the inlet to the outlet plane [9]. Panaseti et al. [5] reported that the shape of the yield surface in plane Poiseuille flow depends only on the shape of the wall and the power-law exponent, while its elevation depends on all parameters. Thus, the width of the unyielded core in a channel of constant width is also constant, despite the pressure dependence of the yield stress, in agreement with the analytical solution.

Fusi and Farina [11] extended their method in Ref. [9] to time-dependent axisymmetric flows. In this geometry, the zero-order approximation leads to a system formed by an integral equation and an algebraic equation for the yield surface and for the plug velocity, respectively. Fusi and Farina [11] focused on the effects of oscillating walls on the flow. The objective of the present work is to study the steady-state axisymmetric Poiseuille flow of a Bingham plastic with pressure-dependent rheological parameters using the method of Fusi and Farina [11]. We are interested in particular in the general case where the growth coefficients α^* and β^* are not equal and thus the unyielded core may be expanding or contracting depending on the relative values of these two parameters.

In Section 2, the various steps of the lubrication method are discussed. These include the non-dimensionalization of the governing equations and the derivation of the zero-order perturbation equations. The advantage of the method is that it leads to closed form solutions for the two velocity components in terms of the pressure distribution and the radius of the central unyielded core, which are functions of the axial distance only. These two functions satisfy a system of a first-order ODE and an algebraic equation. The methods of solving this system are presented in Section 3. These include a numerical pseudospectral method and also a simple perturbation method in terms of the (dimensionless) difference of the two growth coefficients. An analytical solution is also derived for the special case where these coefficients are equal. In Section 4, the results are presented and discussed. Emphasis is given on the effects the dimensionless growth coefficients have on the critical pressure difference required to drive the flow and on the shape of the unyielded core. It is shown, in particular, that the latter expands when $\beta^* > \alpha^*$, contracts when $\beta^* < \alpha^*$, and is cylindrical when $\beta^* = \alpha^*$, in agreement with the aforementioned analytical solution of Ioannou and Georgiou [7]. Finally, the conclusions of this work are summarized in Section 5.

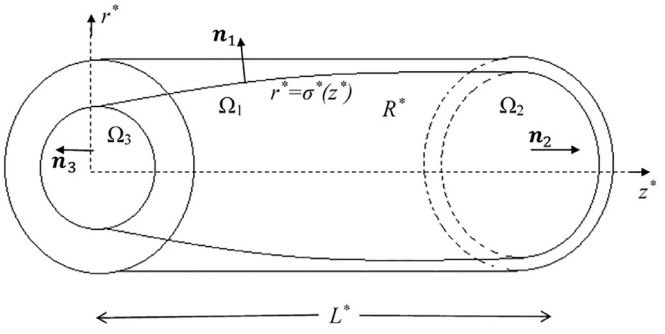

Fig. 1. Schematic of the flow configuration and coordinate system.

2. Lubrication approximation

We consider the steady-state, pressure-driven flow of an incompressible Bingham plastic obeying constitutive Eq. (6) in a long tube of length L^* and constant radius R^*, as illustrated in Fig. 1. A uniform pressure p_{in}^* is applied at the inlet of the tube ($z^* = 0$) while the pressure at the exit plane ($z^* = L^*$) is $p_{out}^* < p_{in}^*$, i.e. the imposed pressure difference is $\Delta P^* = p_{in}^* - p_{out}^*$. Without loss of generality, p_{out}^* is taken equal to the reference pressure p_0^* that appears in Eq. (6), $p_0^* = p_{out}^*$. Assuming that the azimuthal velocity component is zero ($v_\theta^* = 0$) and the flow is axisymmetric (derivatives with respect to θ^* are zero), the velocity vector in cylindrical coordinates is of the form $\mathbf{v}^* = v_r^*(r^*, z^*)\boldsymbol{e_r} + v_z^*(r^*, z^*)\boldsymbol{e_z}$. In the flow of interest (see Fig. 1), the yielded and the unyielded regions are separated by the yield surface $r^* = \sigma^*(z^*)$ for $0 \le z^* \le L^*$ where $0 < \sigma^*(z^*) < R^*$. Hence, the unyielded region extends from the inlet to the outlet, i.e. the plug is not broken. Note that if $\sigma^*(z_c^*) = R^*$ at a point z_c^*, there is no flow since the unyielded region touches the wall and thus the velocity of the unyielded core is zero due to the no-slip boundary condition. For brevity, the symbols $\sigma_{in}^* \equiv \sigma^*(0)$ and $\sigma_{out}^* \equiv \sigma^*(L^*)$ will be used hereafter.

In the yielded region, $D^* \equiv \{(z^*,\ r^*,\ \theta): z^* \in [0,\ L^*], r^* \in [\sigma^*,\ R^*], \theta \in [0,\ 2\pi]\}$, the continuity equation and the z- and r-components of the momentum equation in the absence of external forces, are simplified as follows:

$$\frac{1}{r^*}\frac{\partial(r^* v_r^*)}{\partial r^*} + \frac{\partial(v_z^*)}{\partial z^*} = 0 \tag{7}$$

$$\rho^*\left(v_r^*\frac{\partial v_z^*}{\partial r^*} + v_z^*\frac{\partial v_z^*}{\partial z^*}\right) = -\frac{\partial p^*}{\partial z^*} + \frac{1}{r^*}\frac{\partial(r^*\tau_{rz}^*)}{\partial r^*} + \frac{\partial \tau_{zz}^*}{\partial z^*} \tag{8}$$

$$\rho^*\left(v_r^*\frac{\partial v_r^*}{\partial r^*} + v_z^*\frac{\partial v_r^*}{\partial z^*}\right) = -\frac{\partial p^*}{\partial r^*} + \frac{1}{r^*}\frac{\partial \tau_{rr}^*}{\partial r^*} + \frac{\partial \tau_{rz}^*}{\partial z^*} + \frac{\tau_{rr}^* - \tau_{\theta\theta}^*}{r^*} \tag{9}$$

where ρ^* is the constant mass density. The non-zero components of the rate-of-deformation tensor in the yielded regime are the following:

$$\dot{\gamma}_{rr}^* = 2\frac{\partial v_r^*}{\partial r^*}, \quad \dot{\gamma}_{rz}^* = \frac{\partial v_z^*}{\partial r^*} + \frac{\partial v_r^*}{\partial z^*}, \quad \dot{\gamma}_{zz}^* = 2\frac{\partial v_z^*}{\partial z^*}, \quad \dot{\gamma}_{\theta\theta}^* = 2\frac{v_r^*}{r^*} \tag{10}$$

The non-trivial extra-stress components are given by:

$$\begin{cases} \dot{\gamma}^*_{ij} = 0, & \tau^* \le \tau^*_y(p^*) \\ \tau^*_{ij} = \left\{ \frac{\tau^*_0\left[1+\beta^*(p^*-p^*_0)\right]}{\dot{\gamma}^*} + \mu^*_0\left[1+\alpha^*(p^*-p^*_0)\right] \right\} \dot{\gamma}^*_{ij}, & \tau^* > \tau^*_y(p^*) \end{cases}, \quad ij = rr, rz, zz, \theta\theta \tag{11}$$

where

$$\dot{\gamma}^* = \sqrt{2\left(\left(\frac{\partial v^*_r}{\partial r^*}\right)^2 + \left(\frac{\partial v^*_z}{\partial z^*}\right)^2 + \left(\frac{v^*_r}{r^*}\right)^2\right) + \left(\frac{\partial v^*_z}{\partial r^*} + \frac{\partial v^*_r}{\partial z^*}\right)^2} \tag{12}$$

and

$$\tau^* = \sqrt{\frac{1}{2}\left(\tau^{*2}_{rr} + \tau^{*2}_{zz} + \tau^{*2}_{\theta\theta}\right) + \tau^{*2}_{rz}} \tag{13}$$

The unyielded region $\Omega^* \equiv \{(z^*, r^*, \theta): z^* \in [0, L^*], r^* \in [0, \sigma^*], \theta \in [0, 2\pi]\}$ moves in the z-direction as a solid, i.e. at a constant axial velocity v^*_c. Therefore, in Ω^*:

$$v^*_z = v^*_c \quad \text{and} \quad v^*_r = v^*_\theta = 0 \quad \text{for} \quad 0 \le r^* \le \sigma^*(z^*) \tag{14}$$

In the absence of body forces, the integral balance of linear momentum in Ω^* yields the following equation [11]:

$$\int_{\partial\Omega^*} \rho^*(\mathbf{v}^* \cdot \nabla)\mathbf{v}^* dS^* = \int_{\partial\Omega^*} (-p^*\mathbf{I} + \boldsymbol{\tau}^*) \cdot \mathbf{n} dS^* \tag{15}$$

where $\mathbf{n}$ is the outward unit normal vector to the boundary $\partial\Omega^*$ of Ω^*. Since the core is moving as a solid, the flux of linear momentum through $\partial\Omega^*$ is zero and thus one gets:

$$\int_{\partial\Omega^*} (-p^*\mathbf{I} + \boldsymbol{\tau}^*) \cdot \mathbf{n} dS^* = \mathbf{0} \tag{16}$$

As shown in Fig. 1, the boundary $\partial\Omega^*$ consists of three parts, $\partial\Omega^* = \partial\Omega^*_1 \cup \partial\Omega^*_2 \cup \partial\Omega^*_3$, with the corresponding unit normal vectors given by

$$\mathbf{n}_1 = \frac{\mathbf{e_r} - \sigma^*_z \mathbf{e_z}}{\sqrt{1+\sigma^{*2}_z}}, \quad \mathbf{n}_2 = \mathbf{e_z}, \quad \mathbf{n}_3 = -\mathbf{e_z} \tag{17}$$

where $\sigma^*_z \equiv d\sigma^*/dz^*$. Substituting into Eq. (16) and simplifying one gets the following integral equation:

$$2\int_0^{L^*} \sigma^*\left[\left\{-\sigma^*_z(-p^* + \tau^*_{zz}) + \tau^*_{rz}\right\}\right]_{r^*=\sigma^*(z^*)} dz + \sigma^{*2}_{in} p^*_{in} - \sigma^{*2}_{out} p^*_{out} = 0 \tag{18}$$

2.1. Non-dimensional formulation

The governing equations are rendered dimensionless by scaling z^* by L^*, r^* and σ^* by R^*, $(p^* - p^*_o)$ by $\tau^*_0 L^*/R^*$, v^*_z by $\tau^*_0 R^*/\mu^*_0$, v^*_r by $\tau^*_0 R^{*2}/(L^*\mu^*_0)$, and the extra-stress components by τ^*_o. With these scales, the continuity equation and the two components of the momentum equation become:

$$\frac{1}{r}\frac{\partial(r v_r)}{\partial r} + \frac{\partial v_z}{\partial z} = 0 \tag{19}$$

$$\varepsilon Re\left(v_r\frac{\partial v_z}{\partial r} + v_z\frac{\partial v_z}{\partial z}\right) = -\frac{\partial p}{\partial z} + \frac{1}{r}\frac{\partial(r\tau_{rz})}{\partial r} + \varepsilon\frac{\partial \tau_{zz}}{\partial z} \tag{20}$$

and

$$\varepsilon^3 Re\left(v_r\frac{\partial v_r}{\partial r} + v_z\frac{\partial v_r}{\partial z}\right) = -\frac{\partial p}{\partial r} + \varepsilon\frac{\partial \tau_{rr}}{\partial r} + \varepsilon^2\frac{\partial \tau_{rz}}{\partial z} + \varepsilon\frac{\tau_{rr} - \tau_{\theta\theta}}{r} \tag{21}$$

where

$$\varepsilon \equiv \frac{R^*}{L^*} \tag{22}$$

is the aspect ratio and

$$Re \equiv \frac{\rho^* R^{*2} \tau^*_0}{\mu^{*2}_0} \tag{23}$$

is the Reynolds number.

The components of the dimensionless rate-of-deformation tensor (Eq. (10)) are as follows:

$$\dot{\gamma}_{rr} = 2\varepsilon\frac{\partial v_r}{\partial r}, \quad \dot{\gamma}_{rz} = \frac{\partial v_z}{\partial r} + \varepsilon\frac{\partial v_r}{\partial z}, \quad \dot{\gamma}_{zz} = 2\varepsilon\frac{\partial v_z}{\partial z}, \quad \dot{\gamma}_{\theta\theta} = 2\varepsilon\frac{v_r}{r} \tag{24}$$

As for the non-zero components of the stress tensor we now have

$$\begin{cases} \dot{\gamma}_{ij} = 0, & \tau \le 1 + \beta p \\ \tau_{ij} = \left(\frac{1+\beta p}{\dot{\gamma}} + 1 + \alpha p\right)\dot{\gamma}_{ij}, & \tau > 1 + \beta p \end{cases}, \quad ij = rr,\ rz,\ zz,\ \theta\theta \tag{25}$$

where

$$a \equiv \frac{a^*\tau^*_o L^*}{R^*}, \quad \beta \equiv \frac{\beta^*\tau^*_o L^*}{R^*} \tag{26}$$

are the dimensionless plastic-viscosity and yield-stress growth parameters,

$$\dot{\gamma} = \sqrt{2\varepsilon^2\left[\left(\frac{\partial v_r}{\partial r}\right)^2 + \left(\frac{\partial v_z}{\partial z}\right)^2 + \left(\frac{v_r}{r}\right)^2\right] + \left(\frac{\partial v_z}{\partial r} + \varepsilon\frac{\partial v_r}{\partial z}\right)^2} \tag{27}$$

and

$$\tau = \sqrt{\frac{1}{2}\left(\tau^2_{rr} + \tau^2_{zz} + \tau^2_{\theta\theta}\right) + \tau^2_{rz}} \tag{28}$$

The above equations hold in the yielded domain $D = \{(z, r, \theta) : 0 < z < 1,\ \sigma(z) < r < 1,\ 0 \le \theta < 2\pi\}$. The dimensionless form of Eq. (18) is

$$2\int_0^1 \sigma\left[\left\{-\sigma_z(-p + \varepsilon\tau_{zz}) + \tau_{rz}\right\}\right]_{r=\sigma(z)} dz + \sigma^2_{in} p_{in} - \sigma^2_{out} p_{out} = 0 \tag{29}$$

The system of Eqs. (19)–(21) and (29) is closed by appropriate boundary conditions. At the wall, no-slip and no-penetration conditions are imposed, i.e.

$$v_r = v_z = 0 \quad \text{at} \quad r = 1, \quad 0 \le z \le 1 \tag{30}$$

Along the yield surface, the constant core velocity is imposed:

$$v_r = 0, \quad v_z = v_c \quad \text{at} \quad r = \sigma(z), \quad 0 \le z \le 1 \tag{31}$$

and all components of the rate-of-deformation tensor vanish:

$$\dot{\gamma}_{rr} = \dot{\gamma}_{rz} = \dot{\gamma}_{\theta\theta} = \dot{\gamma}_{zz} = 0 \quad \text{at} \quad r = \sigma(z), \quad 0 \le z \le 1 \tag{32}$$

Regarding the total pressure, this is zero at the exit of the tube ($z = 1$), and equal to the dimensionless pressure difference driving the flow at the tube entrance ($z = 0$):

$$p(r, 0) = \Delta P, \quad p(r, 1) = 0 \tag{33}$$

where $\Delta P \equiv (p^*_{in} - p^*_{out})R^*/(L^*\tau^*_0)$.

2.2. The zero-order approximation

For long tubes, the geometrical aspect ratio ε is a small parameter and if the remaining dimensionless numbers and parameters are of order unity with respect to ε (or smaller) then a lubrication type approximation can be utilized to simplify the governing equations and accompanying auxiliary conditions. Thus, a leading order problem can be formulated provided that:

$$0 < \varepsilon \ll 1, \quad Re, a, \beta, \Delta P \le O(1) \tag{34}$$

For the sake of simplicity, we avoid introducing new symbols for the zero-order variables; hence, hereafter all variables are the zero-order ones. In the yielded region, i.e. for $\sigma(z) \le r \le 1$, all the governing equations and auxiliary conditions at zero-order are simply obtained by setting $\varepsilon = 0$. Hence, at zero order the continuity and momentum Eqs. (19)–(21) become:

$$\frac{1}{r}\frac{\partial(r v_r)}{\partial r} + \frac{\partial v_z}{\partial z} = 0 \tag{35}$$

$$-\frac{\partial p}{\partial z} + \frac{1}{r}\frac{\partial(r\tau_{rz})}{\partial r} = 0 \tag{36}$$

and

$$-\frac{\partial p}{\partial r}=0 \tag{37}$$

It turns out that only the rz-components of the rate-of-deformation and viscous stress tensor are non-zero, i.e.

$$\dot{\gamma}_{rz}=\frac{\partial v_z}{\partial r} \tag{38}$$

with

$$\dot{\gamma}=\left|\frac{\partial v_z}{\partial r}\right|=-\frac{\partial v_z}{\partial r} \tag{39}$$

(the velocity decreases with r) and

$$\begin{cases} \frac{\partial v_z}{\partial r}=0, & \tau\le 1+\beta p \\ \tau_{rz}=-(1+\beta p)+(1+\alpha p)\frac{\partial v_z}{\partial r}, & \tau>1+\beta p \end{cases} \tag{40}$$

The zero-order boundary conditions that accompany the above equations are the same as Eqs. (30)–(33). Finally, the integral Eq. (29) at zero-order becomes:

$$2\int_0^1 \sigma(\tau_{rz}+\sigma' p)_{r=\sigma(z)}dz+\sigma_{in}^2\Delta P=0 \tag{41}$$

where hereafter the prime denotes differentiation with respect to z. Given that $\tau_{rz}=-(1+\beta p)$ at the yield surface ($r=\sigma(z)$), we get

$$2\int_0^1 \sigma\left[-(1+\beta p)+\sigma' p\right]dz+\sigma_{in}^2\Delta P=0 \tag{42}$$

Integrating by parts the second term of the integrand gives:

$$\int_0^1 \sigma\left(1+\beta p+\frac{\sigma p'}{2}\right)dz=0 \tag{43}$$

From Eq. (37), it is deduced that the pressure depends only on z, i.e. $p=p(z)$, and so do the yield-stress τ_y and the plastic viscosity μ. Integrating Eq. (36) with respect to r and demanding that $\tau_{rz}=-\tau_y=-(1+\beta p)$ at the yield surface, we find that

$$\tau_{rz}=\frac{p'}{2}\left(r-\frac{\sigma^2}{r}\right)-(1+\beta p)\frac{\sigma}{r} \tag{44}$$

Combining Eqs. (44) and (40), integrating once again and applying the no-slip boundary condition at the wall ($v_z(r=1,z)=0$), we obtain the following expression for the axial velocity component:

$$v_z(r,z)=\frac{p'}{4(1+\alpha p)}\left(r^2-2\sigma^2\ln r-1\right)-\frac{1+\beta p}{1+\alpha p}(1-r+\sigma\ln r) \tag{45}$$

Therefore, the constant velocity of the unyielded core is

$$v_c=v_z(\sigma,z)=\frac{p'}{4(1+\alpha p)}\left(\sigma^2-2\sigma^2\ln\sigma-1\right)-\frac{1+\beta p}{1+\alpha p}(1-\sigma+\sigma\ln\sigma) \tag{46}$$

As for the radial velocity component, this can be found by integration of the continuity Eq. (35) with respect to r and applying the no-penetration boundary condition ($v_r(r=1,z)=0$):

$$v_r=\frac{1}{r}\int_r^1 \frac{\partial}{\partial z}\left(\xi v_z(\xi,z)\right)d\xi \tag{47}$$

Substituting the axial velocity from Eq. (45) in Eq. (47) and integrating gives an expression for v_r which contains p''. However, we exploit the fact that v_c is constant and take the derivative of Eq. (46) with respect to z. The resulting expression is used to eliminate p'' from the expression for v_r yielding the following expression for the radial velocity:

$$v_r(r,z)=\frac{\left(r^2(\ln(r^2)-1)+1\right)(1-\sigma^2)+(1-r^2)^2\ln(\sigma)}{4r(1+ap)\left(1+\sigma^2(\ln(\sigma^2)-1)\right)} \times\left(1+\beta p+p'\sigma\right)\sigma'+f(r,z)\frac{(\beta-a)p'}{(1+ap)^2},\ \sigma(z)\le r\le 1 \tag{48}$$

where

$$f(r,z)=-\frac{1}{6r}+\frac{r}{2}-\frac{r^2}{3}-\frac{\sigma\left(r^2(1-\ln(r^2))-1\right)}{4r} +\frac{\left((1-r^2)^2+2\sigma^2\left(r^2(1-\ln(r^2))-1\right)\right)(1+\sigma(\ln(\sigma)-1))}{4r(1+\sigma^2\left(\ln(\sigma^2)-1\right))} \tag{49}$$

Eq. (48) reveals a very interesting feature of the flow. For $a=\beta$ the last term in Eq. (48) is zero. Moreover, because $v_r(r=\sigma(z),z)=0$, Eq. (48) gives $\sigma'=0$, which implies that the shape of the interface σ is constant, as indicated also by the numerical results below.

One approach to proceed is by exploiting the fact that v_c is constant, i.e. $\partial v_c/\partial z=0$. Hence, the z-derivative of Eq. (46) is zero which leads to a second-order ODE which contains p, p', p'', σ and σ'. This ODE should be solved together with $v_r(r=\sigma(z),z)=0$ which is a first-order ODE which contains p, p', σ and σ'. Thus, three auxiliary conditions are required to obtain a unique solution. These are the integral Eq. (43) and the two boundary conditions (33):

$$p(0)=\Delta P,\quad p(1)=0,\quad \int_0^1 \sigma\left(1+\beta p+\frac{p'\sigma}{2}\right)dz=0 \tag{50}$$

However, the problem can be further simplified as follows. Eq. (47) evaluated at $r=\sigma(z)$ and multiplied by 2, gives

$$2\int_{\sigma(z)}^1 \frac{\partial}{\partial z}\left(r v_z(r,z)\right)dr=0$$

Since $v_z(r,z)=v_c=\text{constant}$ for $0\le r\le\sigma(z)$ the above equation can be rewritten as:

$$2\int_{\sigma(z)}^1 \frac{\partial}{\partial z}\left(r v_z(r,z)\right)dr+2\int_0^{\sigma(z)} \frac{\partial}{\partial z}\left(r v_z(r,z)\right)dr=\frac{d}{dz}\left(2\int_0^1 v_z r dr\right)=0$$

The quantity inside the parenthesis is simply the dimensionless volumetric flow-rate Q and therefore the above equation implies that Q is constant along the tube (as it should be expected since the fluid is considered incompressible). Since v_z has been found, we can evaluate Q:

$$Q=2\int_0^1 r v_z dr=2\int_0^\sigma r v_c dr+2\int_\sigma^1 r v_z dr=\sigma^2 v_c+2\int_\sigma^1 r v_z dr \tag{51}$$

Carrying out the integration we find Q as a function of σ, p, p' and v_c, i.e. $Q=Q(\sigma,p,p',v_c)$. Eliminating p' by means of Eq. (46) leads to the following algebraic equation:

$$Q=\frac{(1-\sigma)^2}{4\left[1+\sigma^2(2\ln\sigma-1)\right]} \times\left\{(\sigma+1)^2 v_c+\frac{1+\beta p}{3(1+\alpha p)}\left[(1+2\sigma)(1-\sigma^2)+\sigma\ln\sigma(3+2\sigma+\sigma^2)\right]\right\} \tag{52}$$

Eqs. (46) and (52) constitute a system of two equations, the first of which is a first-order ordinary differential equation, which contains p, p', σ and v_c, and the second one is an algebraic equation, with unknowns σ, p, Q, and v_c. Since the ODE is of first order, only one boundary condition is required, but due to the presence of v_c and Q in the equations, two additional auxiliary conditions are needed. Thus, the same boundary conditions given above by Eq. (50) are used.

Solving the system of (46), (52) and (50) gives directly v_c, Q, and $p=p(z)$, $\sigma=\sigma(z)$. Then, the velocity components v_z and v_r are readily calculated by means of Eqs. (45) and (48), respectively. In the next section, the above system of equations is solved using two different methods, an analytical technique and a numerical method, which are discussed next.

3. Methods of solution

Before proceeding with the general solution of the system of Eqs. (43), (48) and (49), recall that an analytical solution of the general flow (without the use of the lubrication approximation) exists when

the two growth coefficients α and β are equal [7]. This is also the case with the lubrication-approximation solution derived above. Indeed, for $\beta = a > 0$, one finds from Eqs. (46) and (48) that the radial velocity vanishes and thus the radius of the unyielded core is constant while $v_z = v_z(r)$ only. More specifically,

$$\tilde{\sigma} = \frac{2a}{\ln(1 + a\,\Delta P)}, \quad \tilde{v}_c = \frac{(\tilde{\sigma} - 1)^2}{2\tilde{\sigma}}, \quad \tilde{Q} = \frac{1}{8\tilde{\sigma}} - \frac{1}{6} + \frac{\tilde{\sigma}^3}{24} \tag{53}$$

while the pressure and the velocity are given by:

$$\tilde{p} = \frac{(1 + a\,\Delta P)^{1-z} - 1}{a}, \quad \tilde{v}_z = (r - 1)\left(1 - \frac{1 + r}{2\tilde{\sigma}}\right), \quad \tilde{v}_r = 0 \tag{54}$$

We point out that the above solution is simply the first term of the Taylor expansion of the analytical solution derived by Ioannou and Georgiou [7] in terms of the aspect ratio ε. The critical pressure gradient, ΔP_c, below which no flow occurs can be found from Eq. (50) as the pressure at which $\tilde{\sigma} = 1$:

$$\Delta P_c = \frac{e^{2a} - 1}{a} \tag{55}$$

For $\beta = a \to 0$, the solution reduces to:

$$\tilde{\sigma} = \frac{2}{\Delta P}, \quad \tilde{v}_c = \frac{\Delta P}{4} - 1 + \frac{1}{\Delta P}, \quad \tilde{Q} = \frac{\Delta P}{16} - \frac{1}{6} + \frac{1}{3(\Delta P)^3} \tag{56}$$

$$\tilde{p} = (1 - z)\Delta P, \quad \tilde{v}_z = (r - 1)\left(1 - \Delta P \frac{1 + r}{4}\right), \quad \tilde{v}_r = 0 \tag{57}$$

and the critical pressure difference is $\Delta P_c = 2$. The above special solutions are the base state for the perturbation solution. Moreover, they are useful in testing the numerical method described below.

3.1. Numerical method

We solve the system of (46), (52) and (50) using a pseudospectral method with Chebyshev orthogonal polynomials. The method is standard, and details can be found in any textbook on spectral methods (see for instance [12]). Briefly, first we map the dimensionless physical domain [0, 1] into the computational domain [−1, 1] by introducing a new independent variable y as $y = 2z - 1 \Leftrightarrow z = (1 + y)/2$. Then, the pressure and the shape of yield surface are represented as:

$$p(y) = \sum_{k=0}^{M} \hat{p}_k T_k(y), \quad \sigma(y) = \sum_{k=0}^{M} \hat{\sigma}_k T_k(y) \tag{58}$$

where $\hat{p}_k$ and $\hat{\sigma}_k$ are the spectral coefficients of p and σ, respectively, M is the total number of coefficients, and $T_k(y) \equiv \cos(k \cos^{-1}(y))$ are the Chebyshev polynomials. This representation generates $2M + 2$ unknowns which, along with v_c and Q, require $2M + 4$ equations. Since the governing equations are strongly non-linear, the computational domain is discretized in $M + 1$ nodes and the discretized form of Eq. (46) at all nodes except from the first one, the discretized form of Eq. (52) at all nodes, and the three auxiliary conditions of Eq. (50), provide $2M + 4$ algebraic equations. This system of non-linear equations is solved using a Newton iterative scheme with an absolute convergence criterion 10^{-12}. The values of M were chosen in the range between 8 and 14 (depending on the magnitude of the parameters); in all cases both p and σ were resolved down to machine accuracy. Before presenting the results, however, we also describe a perturbation method which allows the derivation of an asymptotic solution of the system of interest.

3.2. Asymptotic solution

In order to find an approximate analytical solution of the flow, a perturbation method is employed with the small parameter being the difference between the two growth parameters $\delta \equiv \beta - a$. Then all unknown variables are expanded in standard power series in terms of δ:

$$\chi = \chi_0 + \delta\,\chi_1 + \delta^2 \chi_2 + \ldots \quad \text{as } \delta \to 0, \text{ where } \chi = p, \sigma, v_c, Q \tag{59}$$

The zero-order terms have been already derived above; these are given by Eqs. (50) and (51) for $a = \beta > 0$ and by Eqs. (53) and (54) for $a = \beta = 0$:

$$p_0 = \tilde{p}, \quad \sigma_0 = \tilde{\sigma}, \quad v_{c0} = \tilde{v}_c, \quad Q_0 = \tilde{Q} \tag{60}$$

Substituting expressions (56) and (57) into Eqs. (46), (52) and (50), expanding all quantities suitably, and collecting all terms of the same powers in δ, results in sequence of perturbation problems. We solve analytically the equations at $O(\delta)$ and $O(\delta^2)$. Hence, the asymptotic solution for all variables is found in series form with three terms:

$$\chi_{asym} = \tilde{\chi} + \delta\,\chi_1 + \delta^2 \chi_2, \quad \chi = p, \sigma, v_c, Q \tag{61}$$

However, the analytical solutions at first and second order in δ are too long to be given here. Thus, expressions (61) are mainly used to check and validate the numerical results. In fact, these approximate solutions can also be processed further using series-convergence acceleration techniques, such as Shanks' non-linear transformation [13]. Indeed, an improved approximate solution for all variables is the following:

$$\chi_{acc} = \tilde{\chi} + \frac{\delta\,\chi_1^2}{\chi_1 - \delta\,\chi_2}, \quad \chi = p, \sigma, v_c, Q \tag{62}$$

Comparisons of χ_{acc} with χ_{asym} are performed in the next subsection.

3.3. Code verification

First, we verified the correctness of the pseudospectral method by comparing the numerical results with the analytical solution given by Eqs. (53) and (54). As a test-case we set $\Delta P = 30$ and $a = \beta = 0.1,\ 0.15$ and 0.2. In all cases, the calculated solutions with $M = 10$ were accurate up to 10 significant digits. As a second test-case, we set $a = 0.1$, $\beta = 0.15$, and $\Delta P = 30$ to run the pseudospectral code and get the numerical results χ_{num}; both the pressure and the yield surface were resolved down to machine accuracy using only $M = 12$ spectral coefficients. This indicates that for typical values of the dimensionless parameters the maximum accuracy for all variables is achieved with the pseudospectral code; as such, the solution is considered exact. We also used the analytical asymptotic and improved solutions (χ_{asym}, χ_{acc}, respectively) and calculated the per cent absolute relative errors:

$$\varepsilon_{\chi,asym}(z) = 100\left|1 - \frac{\chi_{asym}(z)}{\chi_{num}(z)}\right|, \quad \varepsilon_{\chi,acc}(z) = 100\left|1 - \frac{\chi_{acc}(z)}{\chi_{num}(z)}\right| \tag{63}$$

where $\chi = \sigma, p$. The calculated errors for the yield surface and the pressure are plotted in Fig. 2. We observe that the error for the asymptotic solution is very low and that its maximum error values (2% for σ, and less than 0.1% for p) are observed at the exit of tube ($z = 1$). This clearly indicates that the perturbation scheme is reliable and that the three-term solutions are excellent approximate solutions to the exact (calculated numerically) solutions.

We also see in Fig. 2 that the improved (accelerated-convergence) solution is slightly more accurate than the asymptotic solution throughout the tube. This indicates that the Shanks transformation for the acceleration of convergence of the three-term asymptotic solution works quite well. The fact that the two solutions are very close confirms the convergence of the results (as already indicated by the low relative errors). It should be emphasized however, that if α is large and $\delta = \beta - a \leq 0.1$ (approximately) the asymptotic and improved solutions do not give physically accepted solutions. Thus, we derive the results using the pseudospectral code and use the asymptotic/improved solutions as an independent check of the numerical results.

4. Results and discussion

Since the fluid is viscoplastic, flow occurs only above a critical value ΔP_c of the imposed pressure difference. As mentioned above, this critical

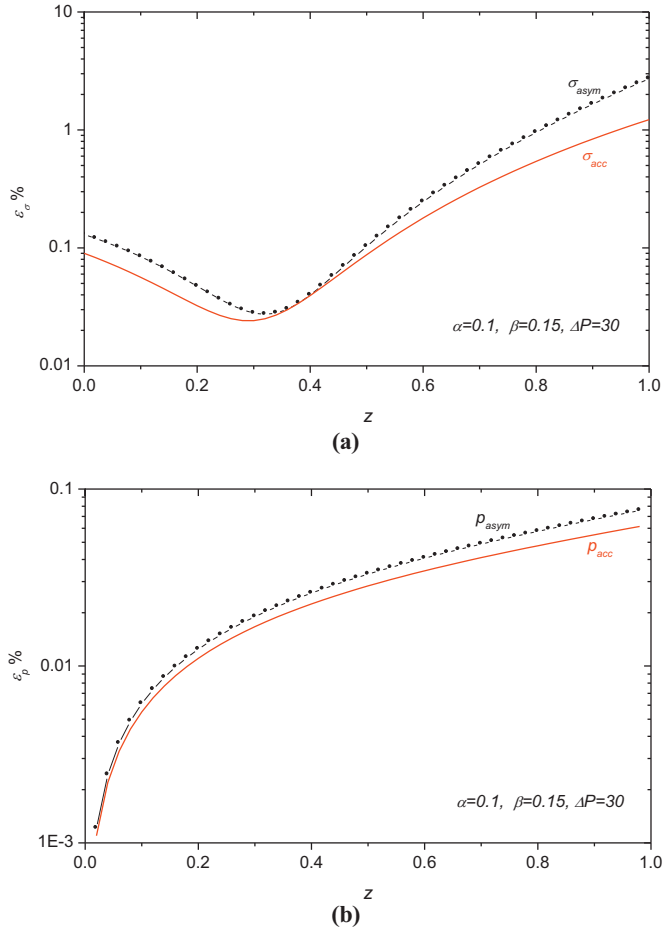

Fig. 2. Absolute relative error for: (a) the shape of the interface and (b) the pressure when $\alpha = 0.1$, $\beta = 0.15$ and $\Delta P = 30$. The dotted lines correspond to the asymptotic solution and the solid ones to the improved (accelerated) solution. The error is calculated based on the numerical solution which is resolved down to machine accuracy.

pressure difference is found as the highest pressure at which the yield surface touches the wall, i.e. $\sigma = 1$ anywhere in the tube. In the previous section, ΔP_c has been derived analytically for the special case where $a = \beta$:

$$\Delta P_c = \begin{cases} \frac{e^{2a}-1}{a}, a = \beta > 0 \\ 2, a = \beta = 0 \end{cases} \quad (64)$$

Obtaining an analytical expression of ΔP_c when $a \neq \beta$ is out of the question. This is thus determined either numerically or asymptotically (see Eqs. (61) or (62), respectively). Representative results are provided in Figs. 3 and 4. It should be noted that in the range of the parameters for which the asymptotic series solution is physically admissible, the agreement between the asymptotic and numerical solutions is excellent. Fig. 3 shows ΔP_c versus the yield-stress growth parameter β for various values of the plastic-viscosity growth parameter, a. In Fig. 4, ΔP_c is plotted versus α for various values of β. The growth parameters a, β should be small, but in order to exaggerate the differences and the effects of the two parameters, we also used values as large as unity.

In Fig. 3, we observe that ΔP_c increases monotonically with β for all values of α. This is expected, since the yield stress increases with β (recall that $0 \le p \le \Delta P$). If now β is fixed, an increase in a enhances the plastic viscosity of the fluid. Even though intuitively the critical pressure difference for a more viscous fluid is expected to be higher, this is not true at high values of β. For fixed values of β higher than 0.3,

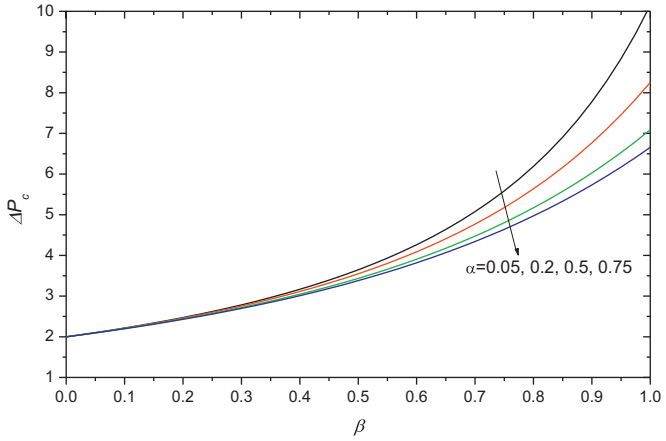

Fig. 3. Effect of the yield-stress growth parameter β on the critical pressure difference, ΔP_c for different values of the plastic-viscosity growth parameter α.

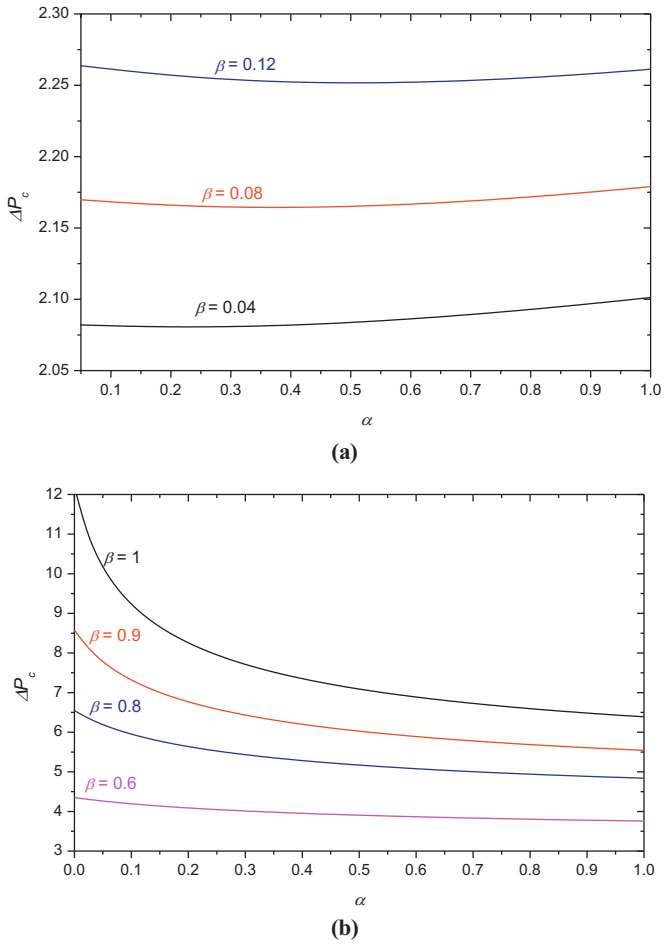

Fig. 4. Effect of the plastic-viscosity growth parameter α on the critical pressure difference, ΔP_c for (a) small and (b) large values of the yield-stress growth parameter β.

ΔP_c decreases with a. The effect of a on ΔP_c is more clearly seen in Fig. 4 where results for low and high values of β are presented. In the former case (Fig. 4(a)), the dependence of ΔP_c on a is weak and ΔP_c passes through a minimum. At higher values of β the variation of ΔP_c with a becomes more significant and the minimum is shifted farther to the right so that ΔP_c appears to decrease monotonically in the range of interest.

Table 1
Indicative values of α and β corresponding to the B34 oil-based drilling fluid studied by Hermoso et al. [2].

T (°C)	Calculated material constants				Dimensionless numbers when $\varepsilon = 10^{-4}$	
	μ_0^* (Pa s)	τ_0^* τ_0 (Pa)	α^* (Pa^{-1})	β^* (Pa^{-1})	α	β
40	0.152	0.144	5.68E−08	1.02E−7	8.18 10^{-5}	1.47 10^{-4}
80	0.028	0.061	2.93E−08	5.41E−8	1.79 10^{-5}	3.30 10^{-5}
100	0.017	0.075	1.65E−08	3.08E−8	1.24 10^{-5}	2.31 10^{-5}
120	0.011	0.022	1.80E−08	1.61E−8	3.96 10^{-6}	3.54 10^{-5}
140	0.01	0.141	2.59E−08	1.27E−8	3.65 10^{-5}	1.79 10^{-5}

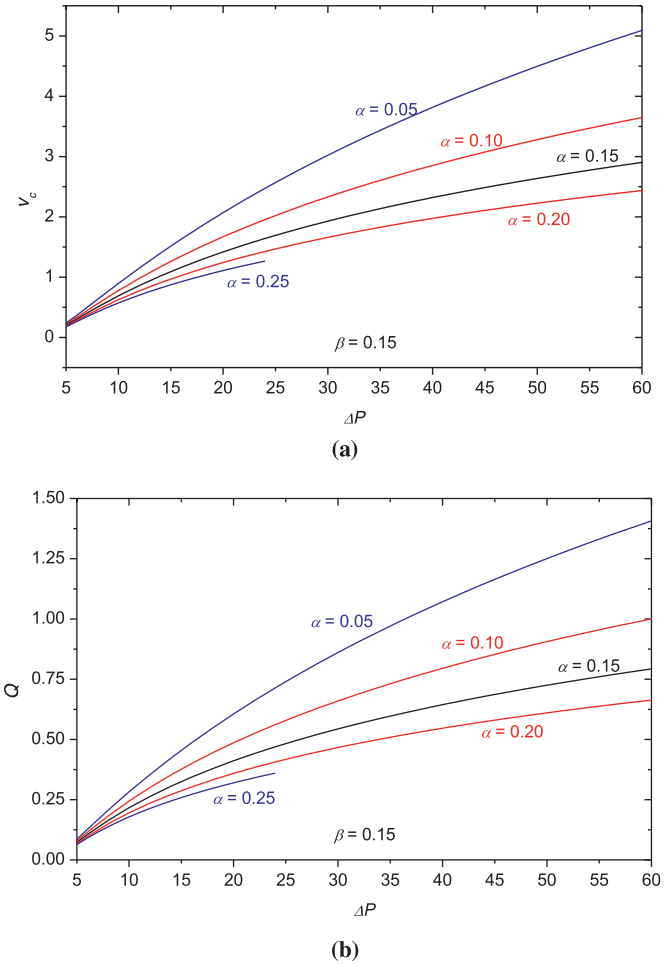

Fig. 5. Variation of (a) the plug-core velocity, v_c and (b) the volumetric flow-rate, Q, with the applied pressure difference ΔP for $\beta = 0.15$ and various values of the plastic-viscosity growth parameter α.

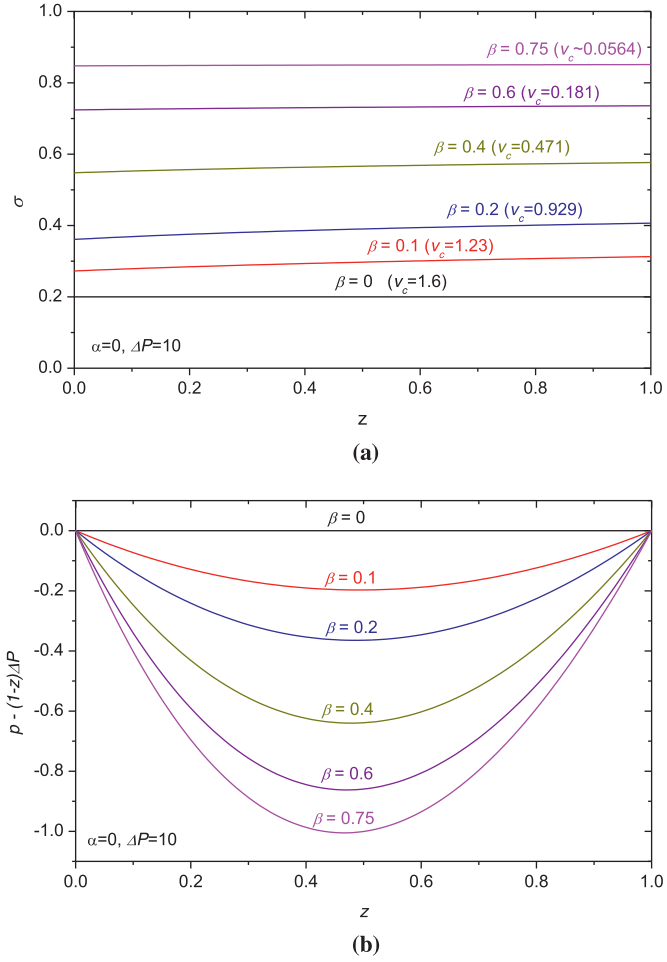

Fig. 6. The effect of the of the yield-stress growth parameter β on (a) the shape of the yield surface, σ, and (b) the modified pressure, $\tilde{p}$, for $\alpha = 0$ (constant plastic viscosity) and $\Delta P = 10$.

It is instructive to resort to available experimental data in order to get a feeling of the magnitudes of α and β. Ioannou and Georgiou [7] determined the values of the rheological parameters corresponding to the B34 oil-based drilling fluid studied at different temperatures and pressures by Hermoso and co-workers [2]. In Table 1, we tabulate the values of α and β at different temperatures, calculated assuming that a representative aspect ratio in oil-drilling is $\varepsilon = 0.0001$. We observe the following: (a) the values of both parameters are of about the same order and well below unity but it should also be noted these would increase if ε is reduced further; (b) at low temperatures $\alpha < \beta$ and at higher temperatures $\alpha > \beta$. In the discussion of the results we intentionally consider higher values of α and β because these may be encountered in other applications and also in order to exaggerate the effects of these two parameters.

In Fig. 5, the velocity of the unyielded core, v_c, and the volumetric flow rate, Q, for $\beta = 0.15$ and various values of a are plotted as functions of the applied pressure difference ΔP in the range $5 \le \Delta P \le 60$, which is above the critical values of ΔP_c. The results for $a = \beta = 0.15$ were calculated using Eqs. (50) and (51). In all cases, both v_c and Q increase monotonically as the imposed pressure difference ΔP is increased. When $a < \beta$, there exists always a solution, at least for the range of ΔP examined here. When $a > \beta$, however, solutions exist only up to a critical value of ΔP, which decreases with the plastic-viscosity growth parameter a (recall that a higher value of a corresponds to a more viscous fluid). A similar observation for the existence of solutions has been reported previously for Newtonian [14] and viscoelastic [15] fluids with pressure-dependent viscosity.

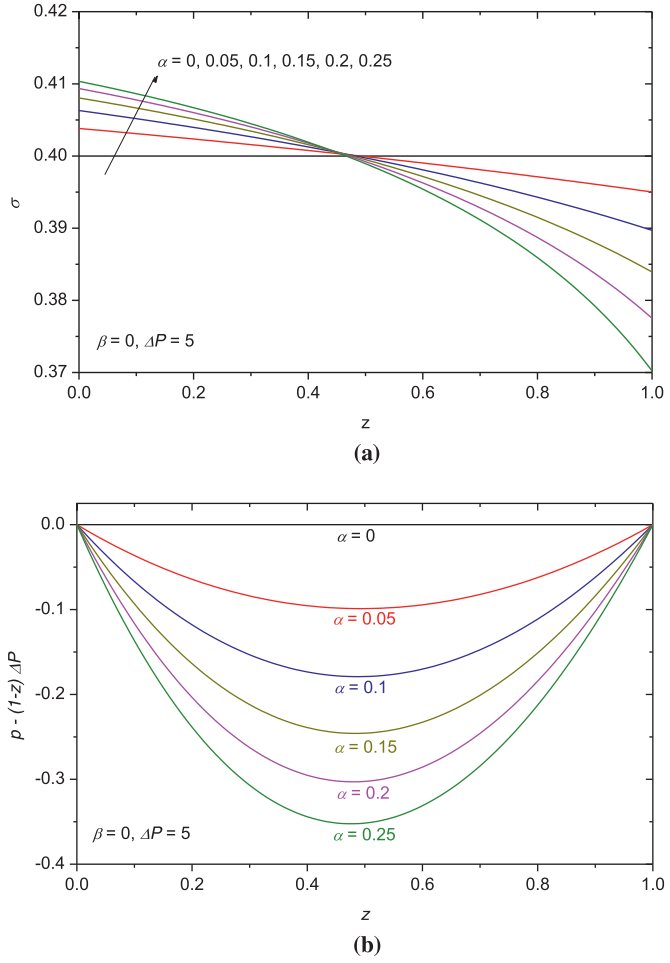

Fig. 7. The effect of the of the plastic-viscosity growth parameter α on (a) the shape of the yield surface, σ, and (b) the modified pressure, $\tilde{p}$, for $\beta = 0$ (constant yield stress) and $\Delta P = 5$.

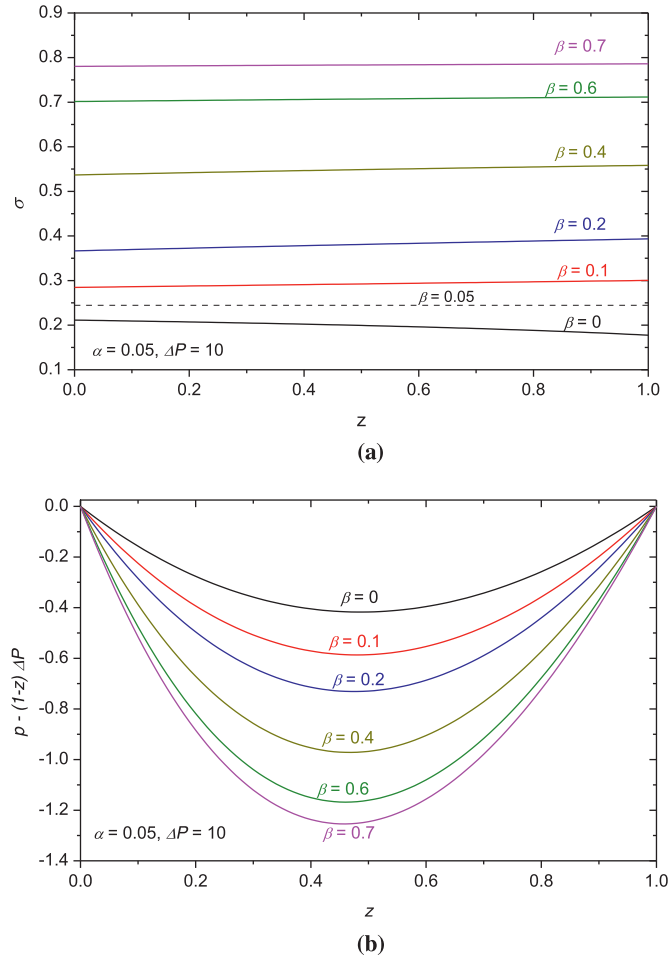

Fig. 8. The effect of the of the yield-stress growth parameter β on (a) the shape of the yield surface, σ, and (b) the modified pressure, $\tilde{p}$, for $\alpha = 0.05$ and $\Delta P = 10$.

We proceed with the effects on the pressure distribution along the tube and the shape of the yield surface σ. In order to focus on the relative changes which may be small, we consider the modified pressure

$$\tilde{p} \equiv p - (1 - z)\Delta P \tag{65}$$

which is actually the deviation from the linear pressure distribution corresponding to the flow of Bingham plastic with constant rheological parameters ($a = \beta = 0$). In Fig. 6, the effect of the yield-stress growth parameter is illustrated for a fluid of constant plastic viscosity ($\alpha = 0$) and $\Delta P = 10$. The values of β were chosen in the range from 0 up to 0.75. Thus, the yield-stress decreases from $\tau_y = 1 + 10\,\beta$ at the entrance to $\tau_y = 1$ at the exit of the tube. For $\beta = 0$, the radius of the unyielded core is constant, given by $\sigma = 2/\Delta P = 0.2$. In all the other cases, a slight increase of σ is observed. The velocity of the unyielded region decreases fast, from $v_c \approx 1.60$ for $\beta = 0$ down to $v_c \approx 0.0564$ for $\beta = 0.75$; a substantial increase of β is then required in order to reduce further the core velocity and to move the yield surface close to the wall. Finally, the corresponding modified pressures are plotted in Fig. 6(b). When $a = \beta = 0$, the modified pressure is zero, as expected from Eq. (57). When $\beta \neq 0$, $\tilde{p}$ is negative, exhibiting a minimum close to the middle of the tube; thus $\tilde{p}'(z_c) = 0$ which implies that $p'(z_c) = -\Delta P$ where z_c is slightly less than 0.5. As expected, $\tilde{p}$ increases in magnitude as β is increased but its shape remains similar.

The effect of the plastic-viscosity growth parameter α for a fluid of constant yield-stress ($\beta = 0$) and $\Delta P = 5$ is illustrated in Fig. 7. As mentioned above, for $a = \beta = 0$ the unyielded core is cylindrical of radius $\sigma = 2/\Delta P = 0.4$, and the modified pressure is zero, i.e. the pressure distribution is linear. In all other cases ($a > \beta = 0$), the radius of the core is not constant, exhibiting a monotonic decrease. It is also interesting to notice that all the yield surface profiles cross at the same distance from the entrance of the tube, slightly before the middle of the tube. As far as the modified pressure is concerned we observe similar patterns as in Fig. 6. It is zero at the entrance and the exit of the tube, and negative elsewhere, showing a minimum, which appears shortly before the middle of the tube at the same position where the yield surfaces cross.

Fig. 8 shows the yield surface and the modified pressure for $\alpha = 0.05$, $\Delta P = 10$ and values of β from 0 up to 0.7. We observe that the shape of the yield surface depends on the relative values of the growth parameters. The radius of the unyielded core decreases monotonically for $\beta < a$, remains constant for $\beta = a$, and increases monotonically for $\beta > a$. The modified pressure profiles are qualitatively the same as those in Figs. 6 and 7.

In Fig. 9 we plotted the yield surfaces for various values of the applied pressure difference, starting from $\Delta P \approx \Delta P_c$ (in which case $\sigma \approx 1$) and increasing ΔP in order to obtain a yield surface as close as possible to the axis of the symmetry of the tube. First, in Fig. 9(a), the results are presented for $a = \beta = 0$ for which $\Delta P_c = 2$; in this case, the radius of the unyielded core is constant, $\sigma = 2/\Delta P$. In Fig. 9(b), results are shown for $a = 0.2, \beta = 0$, i.e. for a fluid with constant yield stress, for which $\Delta P_c = 2$ too. Since $\beta < \alpha$, the radius of the unyielded core is decreasing downstream. In Fig. 9(c), the plastic viscosity is constant, i.e. $a = 0$, while the yield stress varies with the pressure with $\beta = 0.2$; these pa-

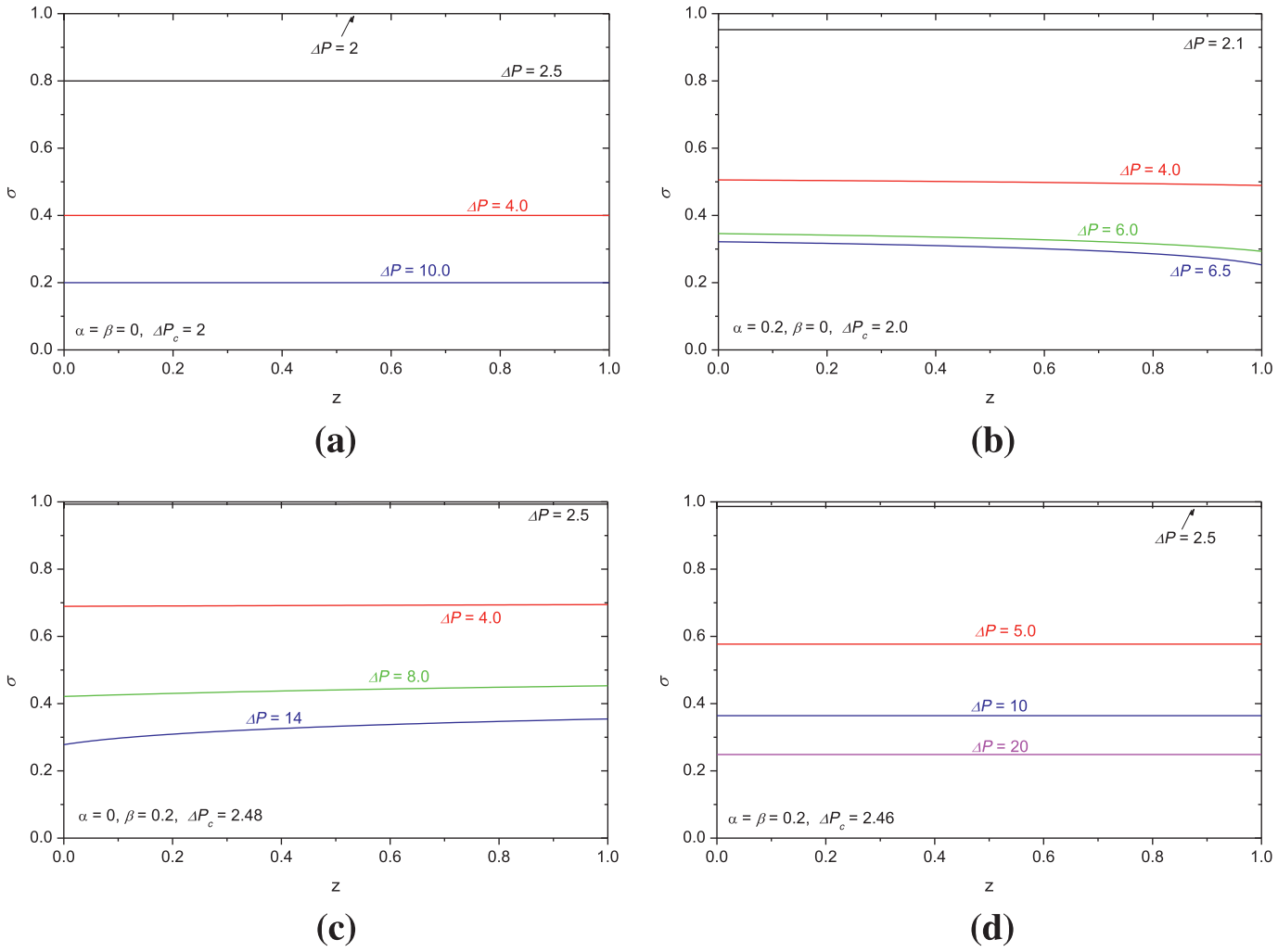

Fig. 9. Yield surfaces for various values of the imposed pressure difference ΔP: (a) $\alpha=\beta=0$; (b) $\alpha=0.2$, $\beta=0$; (c) $\alpha=0$, $\beta=0.2$; (d) $\alpha=\beta=0.2$. The radius σ of the plug core is constant when $\alpha=\beta$, decreasing when $\alpha>\beta$ and increasing when $\alpha<\beta$.

rameters give $\Delta P_c\approx 2.48$. Since $\beta>\alpha$, the radius of the unyielded core is increasing downstream. Last, in Fig. 9(d) the results are shown for $a=\beta=0.2$ which give $\Delta P_c\approx 2.46$.

Finally, in Fig. 10, we plotted the axial velocity profiles in the middle of the tube ($z=0.5$) that correspond to all the cases shown in Fig. 9. For $a=\beta=0$ (Fig. 10(a)) and $a=\beta=0.2$ (Fig. 10(d)) the velocity profile is independent of z but not for $a=0.2$, $\beta=0$ (Fig. 10(b)) and $a=0$, $\beta=0.2$ (Fig. 10(c)). For the lowest applied pressure difference, the radius of the unyielded core tends to unity, i.e. $\sigma=2/\Delta P$, and the magnitude of the velocity tends to zero. As ΔP increases the velocity increases and the radius of the unyielded core moves towards the axis of symmetry, as expected.

4.1. The skin friction coefficient

The skin friction coefficient, C_f, usually referred to as Fanning friction factor [16], is a dimensionless shear stress at the wall of the tube, i.e.

$$C_f \equiv \frac{\tau_w^*}{\rho^* u_s^{*2}/2} \tag{66}$$

where u_s^* is the velocity scale, which in the present work is $u_s^*=\tau_0^* R^*/\mu_0^*$. Substituting and dedimensionalizing τ_w^* by τ_0^* gives:

$$C_f = 2\frac{\mu_0^{*2}}{\rho^*\tau_0^* R^{*2}}|\tau_w| = 2\frac{\mu_0^{*2}}{\rho^*\tau_0^* R^{*2}}\left(\tau_y - \mu\left.\frac{\partial v_z}{\partial r}\right|_{r=1}\right) \tag{67}$$

In the second equality above, we have used that $\tau_w=\tau_{rz}(r=1)$, as well as that τ_y and μ are positive and $\partial v_z/\partial r|_{r=1}$ is negative. The dimensionless group in Eq. (67) is merely the inverse of the Reynolds number (defined in Eq. (23)). Substituting τ_y and μ and evaluating the velocity derivative give:

$$C_f = \frac{2}{Re}\left[\sigma\left(\frac{\sigma p_z}{2}+1+\beta p\right)-\frac{p_z}{2}\right] \tag{68}$$

Since C_f varies with the axial distance, the average skin friction coefficient along the tube is considered. By means of Eq. (50), it turns out that

$$\hat{C}_f \equiv \int_0^1 C_f\, dz = \frac{\Delta P}{Re} \tag{69}$$

It is interesting to note that $\hat{C}_f$ is independent of the growth parameters α and β.

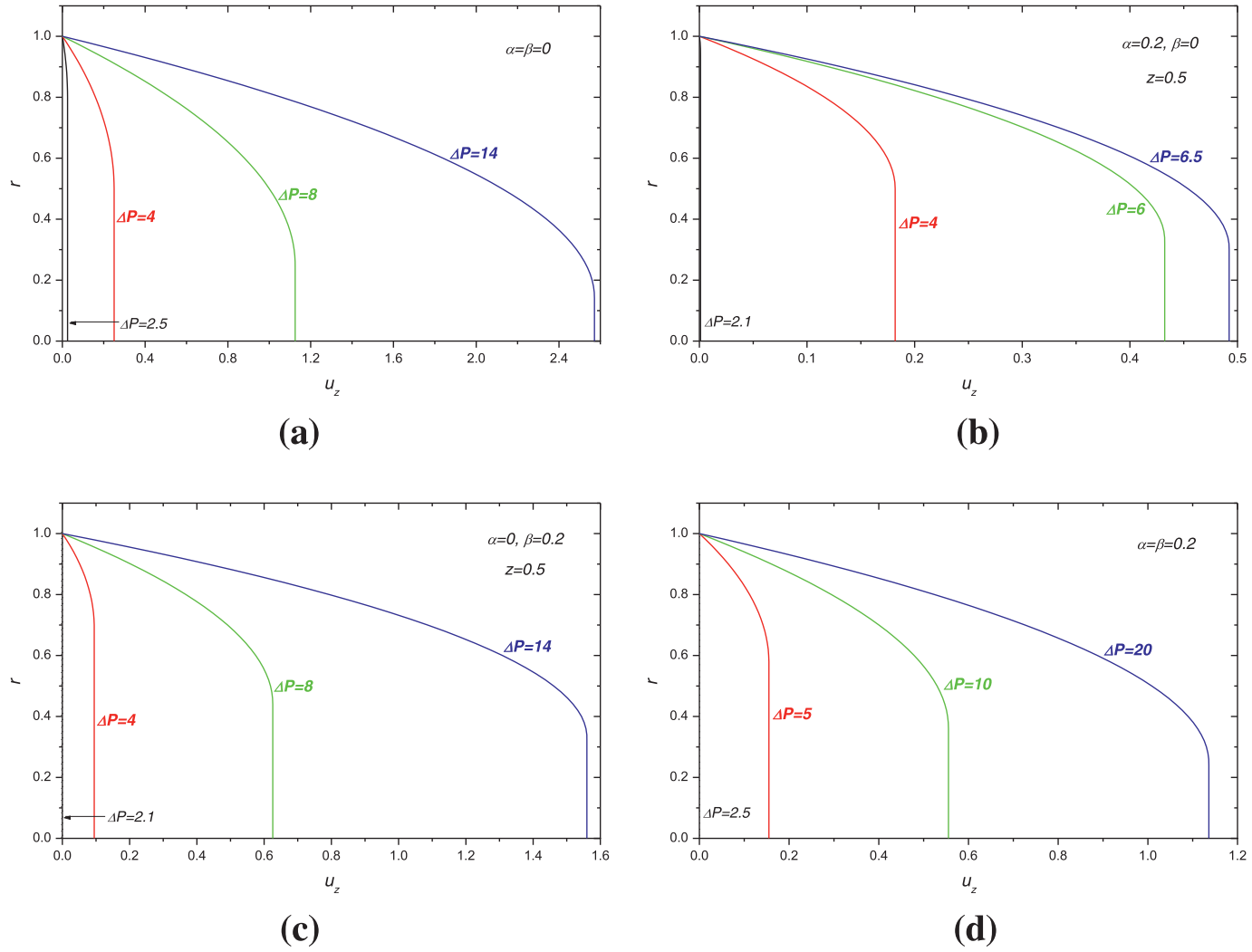

Fig. 10. The axial velocity in the middle of the cylindrical tube ($z = 0.5$) for various values of the imposed pressure difference ΔP: (a) $\alpha = \beta = 0$; (b) $\alpha = 0.2$, $\beta = 0$; (c) $\alpha = 0$, $\beta = 0.2$; (d) $\alpha = \beta = 0.2$.

5. Conclusions

The axisymmetric Poiseuille flow of a Bingham plastic with pressure-dependent rheological parameters has been studied using the lubrication-approximation method of Fusi and Farina [11], which has the advantage of predicting the correct shape of the yield surface at zero order. Both the plastic viscosity and the yield stress have been assumed to vary linearly with the pressure, thus attaining higher values upstream. The perturbation method leads to explicit expressions for the two velocity components in terms of the radius of the unyielded core $\sigma(z)$ and the pressure distribution $p(z)$. These two variables are calculated by solving a system of a first-order ODE and an algebraic equation. This is solved both numerically using a pseudospectral method and by means of simple perturbation method which allows the derivation of some asymptotic results. It is also solved analytically for the special case where the yield-stress growth parameter β is equal to the plastic-viscosity growth parameter α. The effects of these two parameters on the critical pressure ΔP_c required to drive the flow have been studied. While it increases monotonically with β for any value of α, ΔP_c decreases with the plastic-viscosity growth coefficient α at least initially. When β is low, this reduction is weak and ΔP_c passes through a minimum, and then starts increasing with α; for higher values of β, ΔP_c appears to decrease monotonically for the wide range of values considered and the initial reduction is more pronounced. It has also been demonstrated that the shape of the central unyielded core depends on the relative values of α and β. This is contracting when $\beta < \alpha$, expanding when $\beta > \alpha$, and cylindrical when $\beta = \alpha$.

The method of Fusi and Farina [11], exploited here in order to tackle steady-state viscoplastic flow in a cylindrical tube, is more general and can be applied to tubes of non-constant radius, e.g. expanding or contracting tubes, or tubes with a stenosis, or even with oscillating walls. We are thus planning to extend the present work to flows more relevant to industrial applications.

References

[1] E.C. Bingham, Fluidity and Plasticity, McGraw Hill, New-York, 1922.
[2] J. Hermoso, F. Martinez-Boza, C. Gallegos, Combined effect of pressure and temperature on the viscous behaviour of all-oil drilling fluids, Oil Gas Sci. Technol. Rev. IFP Energ. Nouv. 69 (2014) 1283–1296.
[3] W. Herschel, R. Bulkley, Measurement of consistency as applied to rubber-benzene solutions, Proc. Am. Soc. Test Mater. 26 (1926) 621–633.
[4] C. Barus, Isothermals, isopiestics and isometrics relative to viscosity, Amer. J. Sci. 45 (1893) 87–96.
[5] P. Panaseti, Y. Damianou, G.C. Georgiou, K.D. Housiadas, Pressure-driven flow of a Herschel-Bulkley fluid with pressure-dependent rheological parameters, Phys. Fluids 30 (2018) 030701.
[6] Y. Damianou, G.C. Georgiou, On Poiseuille flows of a Bingham plastic with pressure-dependent rheological parameters, J. Non-Newtonian Fluid Mech. 250 (2017) 1–7.

[7] I. Ioannou, G.C. Georgiou, Axisymmetric Poiseuille flow of a Bingham plastic with rheological parameters varying linearly with pressure, J. Non-Newtonian Fluid Mech. (2018), doi:10.1016/j.jnnfm.2018.05.004.
[8] L. Fusi, F. Rosso, Creeping flow of a Herschel-Bulkley fluid with pressure-dependent material moduli, Euro. J. Appl. Math. 29 (2018) 352–368.
[9] L. Fusi, A. Farina, F. Ross, S. Roscani, Pressure-driven lubrication flow of a Bingham fluid in a channel: a novel approach, J. Non-Newtonian Fluid Mech. 221 (2015) 66–75.
[10] I.A. Frigaard, D.P. Ryan, Flow of a visco-plastic fluid in a channel of slowly varying width, J. Non-Newtonian Fluid Mech. 123 (2004) 67–83.
[11] L. Fusi, A. Farina, Peristaltic axisymmetric flow of a Bingham plastic, Appl. Math. Comp. 320 (2018) 1–15.
[12] J.S. Hesthaven, S. Gottlieb, D. Gottlieb, Spectral methods for time-dependent problems, Cambridge University Press, Cambridge, 2007.
[13] D. Shanks, Non-linear transformations of divergent and slowly convergent sequences, *J. Math. Phys.* 34 (1955) 1–42.
[14] A. Kalogirou, S. Poyiadji, G.C. Georgiou, Incompressible Poiseuille flows of Newtonian liquids with a pressure-dependent viscosity, J. Non-Newtonian Fluid Mech. 166 (2011) 413–419.
[15] K.D. Housiadas, An exact analytical solution for viscoelastic fluids with pressure-dependent viscosity, J. Non-Newtonian Fluid Mech. 223 (2015) 147–156.
[16] R.W. Fox, A.T. McDonald, Introduction to Fluid Mechanics, 3th Ed., John Wiley & Sons, Inc., New York (2992).